Thin chalcogenide capillaries as efficient waveguides from mid-infrared to terahertz

Anna Mazhorova, Andrey Markov, Bora Ung, Mathieu Rozé, Stepan Gorgutsa, and Maksim Skorobogatiy*

École Polytechnique de Montréal, Génie Physique, Montréal, Québec H3C 3A7, Canada
**Corresponding author: maksim.skorobogatiy@polymtl.ca*

Received February 29, 2012; revised June 11, 2012; accepted June 26, 2012; posted June 27, 2012 (Doc. ID 163965); published July 25, 2012

We show that chalcogenide glass $As_{38}Se_{62}$ capillaries can act as efficient waveguides in the whole mid-infrared–terahertz (THz) spectral range. The capillaries are fabricated using a double crucible drawing technique. This technique allows to produce glass capillaries with wall thicknesses in the range of 12 to 130 μm. Such capillaries show low-loss guidance in the whole mid-IR–THz spectral range. We demonstrate experimentally that low-loss guidance with thin capillaries involves various guidance mechanisms, including Fresnel reflections at the capillary inner walls, resonant guidance (ARROW type) due to light interference in the thin capillary walls, as well as total internal reflection guidance where very thin capillary walls act as a subwavelength waveguide, which is especially easy to observe in the THz spectral range.

OCIS codes: 060.2390, 230.7370, 300.6495.

1. INTRODUCTION

Chalcogenide glasses have attracted strong interest in a view of optical applications in the near-IR and mid-IR spectral ranges (1–14 μm) [1] due to their relatively low losses and high nonlinearities. Furthermore, chalcogenide glass-based microstructured fibers open many interesting possibilities for a large number of applications in the mid-IR spectral range, where applications in optical sensing [2], supercontinuum generation [3,4], single-mode propagation of IR light [5], and transmission of the CO and CO_2 laser radiation [6,7] have already been demonstrated. We believe that chalcogenide glasses can be also of great interest to the THz spectral range for several reasons. Particularly, as indicated in [8] these glasses offer very high refractive index, and their absorption losses show several regions of relatively low loss and high nonlinearity.

In this paper, we investigate low-loss chalcogenide capillary-based waveguides that operate both in the mid-IR and THz spectral ranges. By exploiting the outstanding performance of chalcogenide glasses in the mid-IR and THz spectral ranges one can envision building fiber-based THz light sources with pumping in the mid-IR.

The main difficulty in designing THz waveguides lies in the fact that almost all materials are highly absorbent in the THz region [9]. Since the lowest absorption loss occurs in dry gases, an efficient waveguide design must maximize the fraction of power guided in the gas. Different types of THz waveguides have been proposed based on this concept [8,10]. Thus, a subwavelength waveguide [10,11] features a core with a size much smaller than the wavelength of light, and as a consequence, a large fraction of the guided light is found outside of the lossy core region. Another type of a low-loss waveguide is presented by the hollow-core fibers featuring a structured cladding that traps the light in the fiber core. As in the case of subwavelength waveguides, hollow-core fibers confine most of the guided light within the low-loss gas region. In the design of hollow-core fibers the main challenge is to ensure high reflection efficiency at the core–cladding interface. Different cladding structures have been developed for the hollow-core-type waveguides, that include metallic reflectors [12–14] and various resonant multilayered dielectric [15–17] reflectors.

Among the hollow-core waveguides with resonant dielectric reflectors the simplest ones are in the form of a capillary [16,17]. In the following we refer to this type of waveguide as pipe waveguides. The structure of the THz pipe waveguide is very simple and consists only of a pipe featuring a thin dielectric layer on its inner surface with a layer size comparable to the wavelength of light. The hollow core defined by the pipe has a diameter that is typically much larger than the wavelength of light. Similar pipe structures have also been demonstrated for guiding IR light [18,19]. The guiding mechanism of pipe waveguides has a resonant nature and is generally referred to as an ARROW type guidance. Finally, we note that ARROW guidance is distinctly different from the total internal reflection (TIR) guidance mechanism employed by the subwavelength-sized low-refractive-index discontinuity waveguides [20].

In this paper, we detail using thin chalcogenide glass $As_{32}Se_{68}$ capillaries for guidance in the mid-IR and THz spectral regions.

The guiding mechanism in such capillaries has been well described [21,22]. In the THz spectral range they guide via total internal reflection, while in the mid-IR spectral range guiding mechanism is dictated by the antiresonant reflection conditions where the wall of the capillary acts as a Fabry–Perot resonator [16,17]. At the resonant frequencies, the light leaks through the capillary wall and leaves the waveguide. While under the antiresonant condition, the field is strongly reflected by the capillary wall leading to field confinement in the hollow core. Transmission windows are delimited by the resonant frequencies that can be accurately predicted. Only few percent of power is guided in the material and most of the guiding is in the air. The attenuation in the transmission bands usually is remarkably lower than in the bulk material. In the silica pipes at THz frequencies, the attenuation coefficient can be lower than 0.03 cm^{-1} (13.62 dB/m), whereas silica absorption is around 2 cm^{-1} [21,23], leading to an attenuation coefficient of the propagated field significantly lower than the material absorption coefficient. However, an increase of the losses is unavoidable owing to wall-thickness variations in the fabricated capillaries.

Notably, the same chalcogenide capillary can act as an ARROW waveguide in the mid-IR and as a TIR waveguide in THz.

2. GLASS SYNTHESIS AND CAPILLARIES FABRICATION

The capillaries in this work are drawn under pressure from the chalcogenide glass melt by using a double crucible drawing technique [6,23,24]. The wall thickness of the glass capillary is controlled during drawing using temperature and pressure, thus allowing fabrication of very thin capillaries with wall thickness ranging in the 12 μm [Fig. 1(b)]–130 μm [Fig. 1(a)].

Chalcogenide glasses are typically synthesized from pure chemical elements, where bulk samples of vitreous arsenic chalcogenides of optical grade are produced by solidification of the glass-forming melt [25]. We here use $As_{38}Se_{62}$ glass. This composition was chosen because of its higher stability against crystallization during the drawing compared to As_2Se_3. An 80 g glass preform was prepared from the pure materials (Se: 99.999% 5N and As: 99.999% 5N). The compounds are introduced in a chemically cleaned and dried silica ampoule. The ampoule was then evacuated using a diffusion vacuum pump to the pressure of 5×10^{-7} mbar and placed into a rocking furnace where the glass is melted at temperatures above 600 °C. In the next step, the glass is first slowly cooled down to 450 °C and then quenched in cold water in order to solidify the glass-forming melt. The obtained glass rod is then annealed overnight under a temperature close to the glass transition temperature T_g ($T_g = 165\,°C$) so as to reduce inner stress caused by the quenching. The chalcogenide glass rod is then removed from the silica ampoule and inserted into the quartz-based double crucible.

Traditionally, the double crucible setup is used to draw step index fibers in which both volumes of the double crucible contain core and clad glasses with different refraction indices

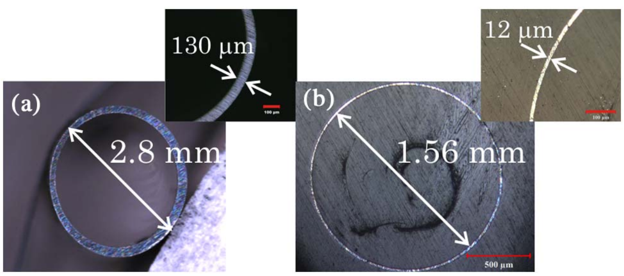

Fig. 1. (Color online) Fabricated chalcogenide glass capillaries with different wall thickness in the range of (b) 12 μm to (a) 130 μm by double crucible glass drawing technique. To perform an imaging of thin wall capillaries, such as capillary with 12 μm walls shown at (b), they were glued in epoxy and then polished.

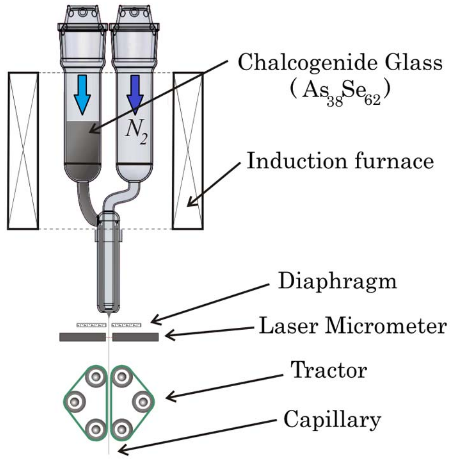

Fig. 2. (Color online) Setup for drawing capillaries using the double-crucible method.

(i.e., different chemical compositions) in order to yield either a multimode or single-mode fiber, depending on the core size in the final fiber [25]. A schematic of our drawing tower with the double-crucible method is presented in Fig. 2. In our case, the volume of the crucible designed for the fiber core remains empty while the clad crucible contains the synthesized $As_{38}Se_{62}$ glass. The entire chamber with the double crucible is purged at 50 °C overnight with a constant flow of N_2 to avoid O_2 and dust particles in the heated zones.

The temperature slowly increases from the bottom to the top of the crucible. In the higher zone, at 400 °C the glass starts to melt and flows down to the cooler zones (~295 °C) along the crucible, thus the viscosity of the melt in the lower zones is higher, which enables us to have a slower and more controllable flow. At the tip of the double crucible, a drop of glass is formed and as it goes down by gravity, the fiber is drawn like in a conventional fiber drawing tower. As soon as the drop reaches the tractor, it is pulled down with a controlled speed; meanwhile, the pressure in the core crucible is increased in order to form a capillary. By varying the drawing conditions, such as tractor speed and pressure in the core, numerous dimensions of capillaries and wall thicknesses have been obtained.

In case of capillaries with thin walls (around 20 μm), the mechanical stability of the drawn fiber can sometimes be low. If the walls of the capillary are very thin, they can be easily crushed due to squeezing within mechanical parts of the tractor during the fabrication or later with fingers. For the capillaries with the outer diameter of 2 mm and wall thickness 80 μm minimal bending radius is around 15 cm, which demonstrates good mechanical strength. However, capillaries with thinner walls are still very fragile and are almost impossible to be bent.

3. ABSORPTION LOSS OF THE $AS_{38}SE_{62}$ GLASS

Figure 3 presents the absorption loss of the $As_{38}Se_{62}$ rod-in-the-air fiber with diameter 350 μm in the 1–12 μm spectral range obtained by the cut-back measurement from 1 m to 30 cm. The minimum of attenuation is about 2.89 dB/m at 3.85 μm. One can notice that the absorption bands due to hydrogen impurities (O-H and H_2O) are important compared

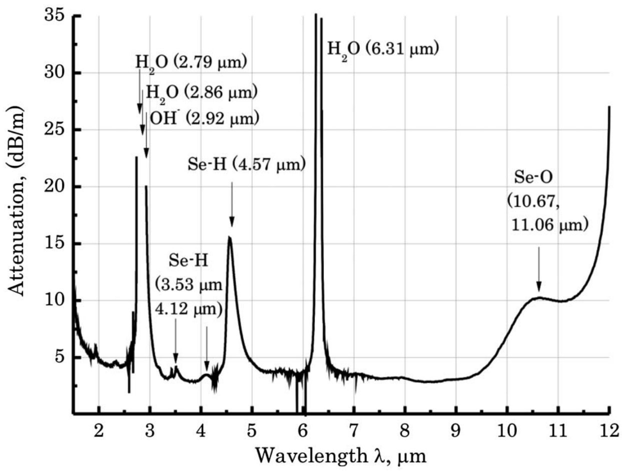

Fig. 3. Absorption loss of the $As_{38}Se_{62}$ rod with diameter 350 μm. Absorption bands in the 3–5 μm spectral range corresponds to impurity absorptions due to SeH bond at 3.53, 4.12, 4.57 μm. Also, strong absorption bands at 2.7–2.93 μm and 6.31 μm are due to OH—group and water.

with the Se-H band at 4.5 μm. Such impurities can be in principle removed by using standard static or dynamic distillation processes that require complex glassware [25–27]. Increase of the optical losses in the 10–12 μm spectral region is usually explained by the effect of the oxygen impurity (Se-O, arsenic oxides) [28–30].

In the mid-IR spectral range we have used Sellmeier fit of the real part of the refractive index versus wavelength [31]:

$$n(\lambda) = [1 + \lambda^2 \cdot (A_0^2/(\lambda^2 - A_1^2) + A_2^2/(\lambda^2 - 19^2) + A_3^2/(\lambda^2 - 4 \cdot A_1^2))]^{1/2}, \tag{1}$$

where $A_0 = 2.234921$, $A_1 = 0.24164$, $A_2 = 0.34744$, $A_3 = 1.308575$, resulting in the values in the range 2.76–2.8. $As_{38}Se_{62}$ glass in the 2–12 μm range features relatively small absorption losses 0.01 cm^{-1}, while showing complex and generally nonmonothonic growth of the absorption losses with the subsequent increase of the wavelength [6] in the 4–18 THz spectral range.

Refractive index of the chalcogenide glass in THz spectral region was measured in-house using THz- time-domain spectroscopy (TDS) setup. Real part of the refractive index was found to be nearly constant in the whole 0.1–2.5 THz range and its value is approximately 3.12. Imaginary part of the refractive index in the 0.1–2.5 THz spectral range was found to increase quadratically with frequency and can be estimated as $1.9\omega + 50.9\omega^2$, where ω is the frequency in THz.

4. RESULTS AND DISCUSSION

As we have mentioned earlier, the guiding mechanism of the leaky core modes in the capillary waveguide (chalcogenide glass tube) is similar to that of the antiresonant optical waveguides (ARROWs) [16,17,21,22], and can be simply described by considering the capillary wall as a Fabry–Perot étalon [Figs. 4(a) and 4(b)]. Close to the resonance frequencies [Eq. (2)], there is almost no reflection from the tube walls and, consequently, light not well confined inside the capillary. On the other hand, under the antiresonant condition considerable reflections at the inner side of the tube result in the strong light confinement (waves bounce back and forth inside of the capillary).

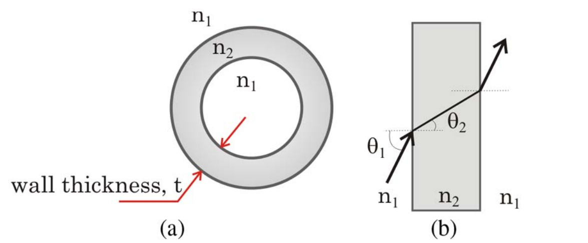

Fig. 4. (Color online) (a) Profile of the capillary waveguide; (b) Fabry–Perot etalon.

The resonant frequencies of the tube wall are given by the condition of the constructive interference between the multiple reflections of light between the two refracting surfaces of the wall [Fig. 4(b)], where n_2 and n_1 denote the refractive indices of chalcogenide glass and air, respectively; θ_1 and θ_2 are incident and reflected angles with respect to the interface normal, respectively; t is the wall thickness of the capillary. Then, frequencies at which tube wall becomes virtually transparent to the incident light are given by

$$f_m = \frac{mc}{2 \cdot n_2 \cdot t \cdot \cos\theta_2} = \frac{mc}{2 \cdot n_2 \cdot t \cdot \sqrt{1 - (n_1 - n_2)^2}} = \frac{mc}{2t\sqrt{n_2^2 - n_1^2}}, \tag{2}$$

where c is the speed of light in vacuum, m is an integer and we suppose that radiation angle of incidence is grazing ($\theta_1 = \pi/2$), which is true for the capillaries with diameters much larger than the wavelength of light. These resonances result in the appearance of the periodic minima in the capillary transmission spectrum. The bandwidth of the transmission windows is given by

$$\Delta f = f_{m+1} - f_m = \frac{c}{2t\sqrt{n_2^2 - n_1^2}}. \tag{3}$$

Or in terms of wavelength:

$$\Delta\lambda = \lambda_m - \lambda_{m+1} = \frac{\lambda_m \cdot \lambda_{m+1}}{2t\sqrt{n_2^2 - n_1^2}}. \tag{4}$$

Modal characteristics of the pipe waveguides have been also numerically investigated using full-vector transfer matrix theory and the finite element method (Comsol software). For each capillary the attenuation constants of the lowest 12 modes of the waveguide have been calculated. The fundamental HE_{11} ARROW mode has the highest coupling coefficient with an incident linearly polarized Gaussian beam and has the lowest attenuation constant. The resonance positions and the bandwidth of the transmission windows are the same for the fundamental and higher-order modes. Modal indices of the higher-order modes are somewhat lower than that of the fundamental mode. Within the ray-optics approach, this means that the higher-order modes propagate at a higher inclination angle (with respect to the propagation axis) than

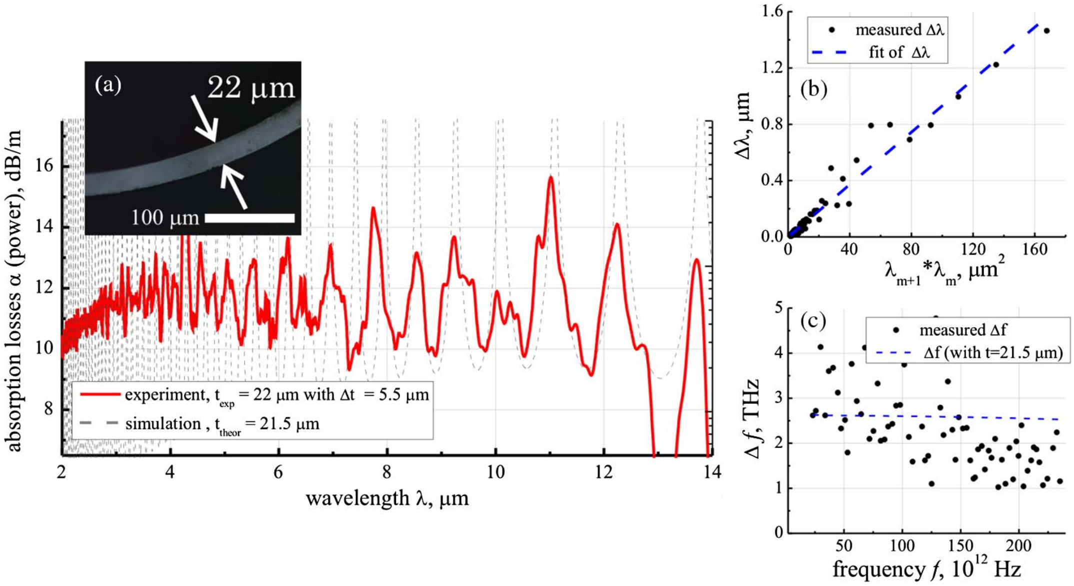

Fig. 5. (Color online) (a) Absorption losses of capillary with 22 μm average wall thickness in spectral range from 2–14 μm, measured with the cut-back method. (b) Measured period of the resonances $\Delta\lambda$ as a function of product of two consecutive resonance wavelengths $\lambda_{m+1} * \lambda_m$ (μm^2) from Fig. 5(a) of absorption losses; (c) Measured period of the resonances Δf as a function of frequency. Blue dashed line is the experimental fit of the resonances, which gives the wall thickness value of $t_{\text{fit}} = 21.2 \pm 4.8$ μm, which is in a good agreement with measured optical microscope wall thickness $t = 22.1 \pm 5.5$ μm.

the fundamental mode; the modes with higher angles at the core–cladding interface incur larger attenuation constants. Also, we note that modes of a fiber only with angular momentum equal to 1 can be excited by the incoming (centered) Gaussian beam due to symmetry considerations. Finally, distribution of the transverse E–field components $E_{\text{output}} = (E^x_{\text{output}}, E^y_{\text{output}})$ at the output facet of a fiber of length L_w is modeled as a coherent superposition of the $N = 12$ lowest loss guided modes:

$$\vec{E}_{\text{output}}(x, y, \omega) = \sum_{m=1}^{N} C_m \cdot \vec{E}_m(x, y, \omega) \cdot \exp\left(i\frac{\omega}{c} \cdot n_{\text{eff},m} \cdot L_w\right) \times \exp\left(-\frac{\alpha_m L_m}{2}\right), \tag{5}$$

where $\vec{E}_{\text{output}} = (E^x_{\text{output}}, E^y_{\text{output}})$ stands for the transverse field components of the m-th guided mode. The variables α_m and $n_{\text{eff},m}$ denote respectively the power loss coefficient and the real effective refractive index of the m-th mode at a given frequency ω. The variable C_m refers to the standard normalized amplitude coupling coefficients computed from the overlap integral of the respective flux distributions of the m-th mode with that of the input beam [32].

Transmission measurements were performed in two spectral ranges: in mid-IR from 1.5 to 14 μm by the Fourier transform infrared technique (FTIR) using a modified ABB FTLA2000 Fourier transform IR spectrometer, and in THz spectral range from 0.1 up to 3 THz by a THz-TDS setup. The setup consists of a frequency-doubled femtosecond fiber laser (MenloSystems C-fiber laser) used as the pump source and two identical GaAs dipole antennae used as source and detector of a spectrum ranging from ~0.1 to 3 THz. Contrary to the standard THz-TDS setup where the configuration of parabolic mirrors is static, the utilized setup has mirrors mounted on translation rails. This flexible reconfiguration facilitates mirrors placement, allowing measurement of waveguides up to 50 cm in length without realigning the setup (for more details see [33]).

A. Capillaries in Mid-IR Spectral Range

In the mid-IR spectral range, the dominant guidance mechanism is the antiresonant reflection from the capillary walls with the highest fraction of power concentrated inside the hollow core.

Very thin chalcogenide capillaries with wall thickness below 25 μm and outer diameter 1–2 mm guide very well the mid-IR radiation with losses from 7 to 16 dB/m depending on the wavelength. Figure 5(a) illustrates absorption losses of capillary with average wall thickness of 22 μm in the spectral range from 2–14 μm, measured with the cut-back method by the FTIR technique. The results of the transfer matrix calculation for the fundamental mode are shown as a dashed line. The comparison of the theoretical results with the experimental data shows that for such capillaries the positions of the absorption minimums and the widths of the transmission bands can be well described by taking into account only a single fundamental HE_{11} mode. Figure 5(b) shows measured periods of the resonances $\Delta\lambda = \lambda_{m+1} - \lambda_m$ (difference between the two adjacent absorption loss maxima λ_{m+1}, λ_m) as a function of the product of two consecutive resonance wavelengths $\lambda_{m+1} * \lambda_m$ (μm^2). The blue-dashed lines in the Figs. 5(b) and 5(c) are the theoretical fits of the experimental data using Eqs. (3) and (4). From these fits we find that to explain the position of the transmission minima capillary, wall thickness has to have a value of $t_{\text{fit}} = 21.2 \pm 4.8$ μm, which is in good agreement with measurements corresponding to the wall thickness retrieved with the optical microscope $t = 22.1 \pm 5.5$ μm [inset in the Fig. 5(a)].

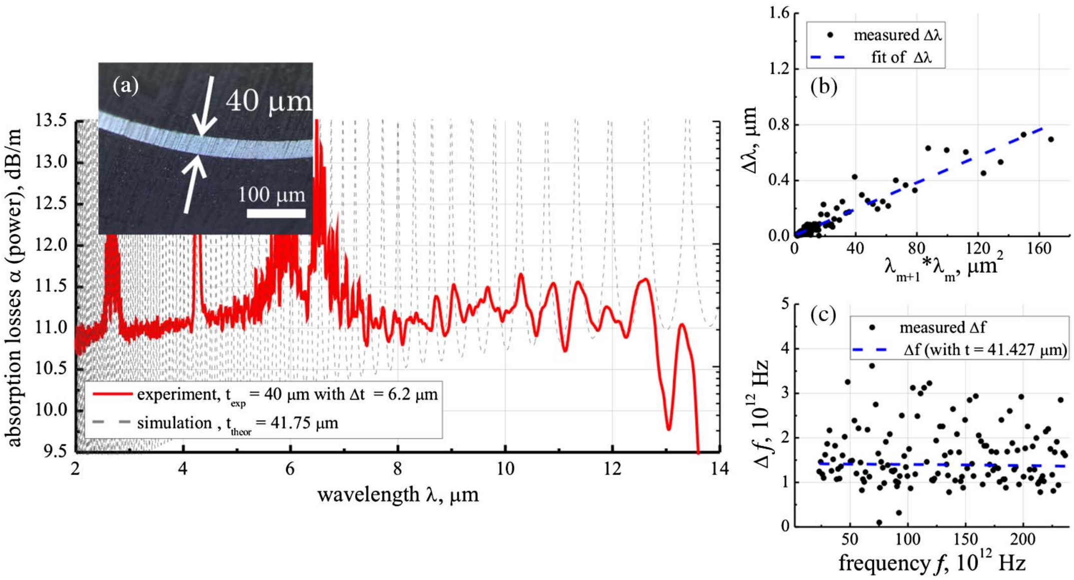

Fig. 6. (Color online) (a) Absorption losses of the capillary with average wall thickness 40 μm in the spectral range 2–14 μm. (b) Measured period of the resonances $\Delta\lambda = \lambda_{m+1} - \lambda_m$ (difference between the two adjacent absorption loss maxima λ_{m+1}, λ_m) as a function of product of two consecutive resonance wavelengths $\lambda_{m+1} * \lambda_m$ (μm^2) from Fig. 6(a) of absorption losses. (c) Measured period of the resonances Δf as a function of frequency. Blue line is the experimental fit of the resonances, which gives the wall thickness value of $t_{\rm fit} = 41.4 \pm 5.6$ μm, which is in a good agreement with measurements via the optical microscope $t = 40.1 \pm 6.2$ μm.

Figure 6(a) illustrates absorption losses of capillary with average wall thickness of 40 μm within the spectral range from 2–14 μm. Compared to the thin capillaries, spectral oscillations in the transmission spectrum of the twice as thick capillary are much less pronounced, especially at shorter wavelengths. Weak oscillations are still visible between 8 and 13 μm. Figure 6(b) shows measured period of the resonances $\Delta\lambda = \lambda_{m+1} - \lambda_m$ (difference between the two adjacent absorption loss maxima λ_{m+1}, λ_m) as a function of product of two consecutive resonance wavelengths $\lambda_{m+1} * \lambda_m$ (μm^2) from Fig. 6(a) of absorption losses. Theblue-dashed lines are the experimental fit of the resonances, which gives a wall thickness value of $t_{\rm fit} = 41.4 \pm 5.6$ μm, that is in good agreement with measurements with the optical microscope observation: $t = 40.1 \pm 6.2$ μm [inset of Fig. 6(a)]. The absorption losses measured using capillaries samples are typically consistently higher than the losses of the rods of the same material. We believe that it can be explained by the surface roughness of the capillaries. The scales of this roughness and the nonuniformity of the capillaries wall thickness can be comparable with the wavelength causing the dissipation of the transmitted power.

When using even thicker capillaries, the spectral contrast between minima and maxima in the mid-IR transmission spectrum decreases, and in very thick capillaries with wall thicknesses above 100 μm, the oscillations are not detectable with the FTIR technique. Capillaries tend to show a featureless spectrum with $\sim$15 dB/m losses. Figure 7(a) illustrates

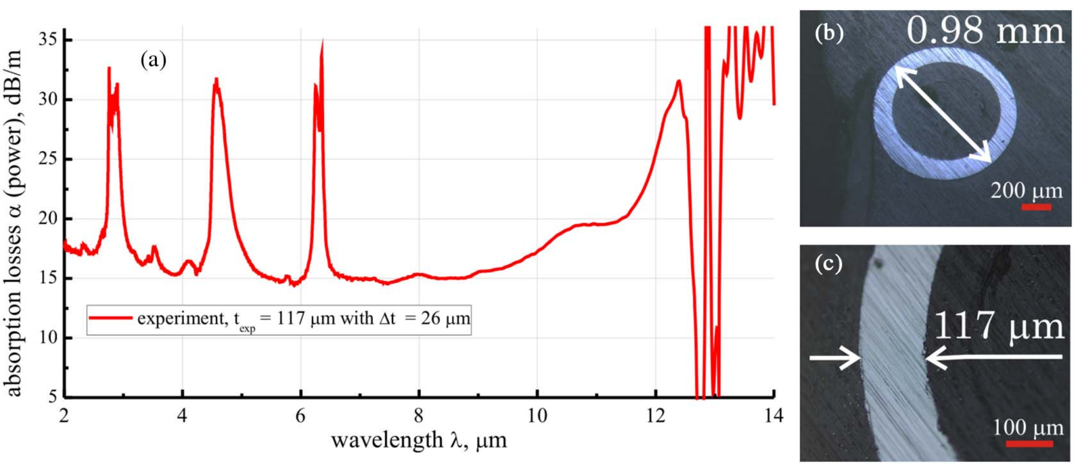

Fig. 7. (Color online) (a) Absorption losses of the capillary in the spectral range 2–14 μm, it tends to show a featureless spectrum with $\sim$5 dB/m losses. (b) and (c) optical micrographs of the capillary with outer diameter of 0.98 mm and averaged wall thickness 117 μm.

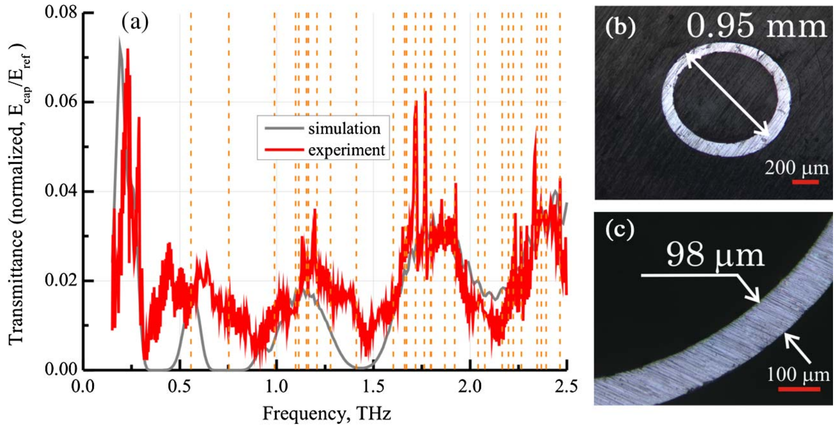

Fig. 8. (Color online) (a) Transmittance by field of the effectively single mode 50 cm long capillary with 98 μm average wall thickness and 0.95 mm diameter in the spectral range between 0.1–2.5 THz. At lower frequencies ($\omega < 0.3$ THz) guidance mechanism is of TIR type with losses ~44 dB/m, while at higher frequencies ($\omega > 0.3$ THz) guidance is of ARROW type with total losses ranging in the 58–93 dB/m range, depending on the operation frequency. (b) and (c) Optical micrographs of the capillary used in the experiments with outer diameter of 0.95 mm and averaged wall thickness 98 μm. Orange dashed lines correspond to the positions of the water lines in the THz spectrum.

absorption losses of the capillary 0.98 mm in diameter with average wall thickness 117 μm in the spectral range 2–14 μm [Figs. 7(b) and 7(c)].

B. Capillaries in the THz Spectral Range

In the THz spectral range, the thicker capillaries (~100 μm) show clear antiresonant guidance with periodic minima and maxima as a function of frequency. Figure 8(a) illustrates the transmittance through a 50 cm long capillary with wall thickness $t = 98$ μm and diameter 0.95 mm with total losses by power (coupling and transmission) ranging from 58 to 93 dB/m depending on the frequency.

Numerical simulations show that a 50 cm long chalcogenide capillary of 0.95 mm diameter and 98 μm thickness operates in the effectively single-mode regime, while higher-order modes contribute only to small oscillations in the fiber transmission spectrum due to their higher attenuation constants.

Particularly, at low frequencies (<0.3 THz) the only guided mode supported by a capillary is a TIR mode where a thin-walled capillary acts as a subwavelength waveguide [see Fig. 9(b)]. In this case, capillary wall thickness is much smaller than the wavelength of light, while the capillary diameter is comparable or smaller than the wavelength of light. At higher frequencies (>0.3 THz), the waveguide is again effectively single mode with the principal mode being the ARROW mode mostly concentrated in the fiber core [see Fig. 9(a)]. In this case, capillary wall thickness is comparable to the wavelength of light, while the capillary diameter is much larger than the wavelength of light. Longitudinal energy flux distributions for the ARROW and TIR modes computed at frequencies 0.57 THz and 0.18 THz are shown in Figs. 9(a) and 9(b). The operation frequency for the ARROW mode is chosen to be in the center of a transmission band, so that the fiber fundamental mode power is confined almost entirely inside of the capillary hollow core [see Fig. 9(a)]. In contrast, the TIR mode is guided mostly outside of the capillary with only a small fraction of power inside the hollow core [see Fig. 9(b)]. The capillary wall thickness of 91 μm (compared to 98 μm measured thickness) was taken in numerical simulations for the best match of the positions of the transmission peaks with the experimental data. This difference can be explained by the nonuniformity of the capillaries, their average thickness can differ slightly from the value measured on their facets. Alternatively, it can be explained by an inaccuracy in measurement of the refractive index of the chalcogenide glass. Both these values are key parameters in the equation which defines the positions of minimal and maximal transmittance of the capillary when it guides through the antiresonant mechanism.

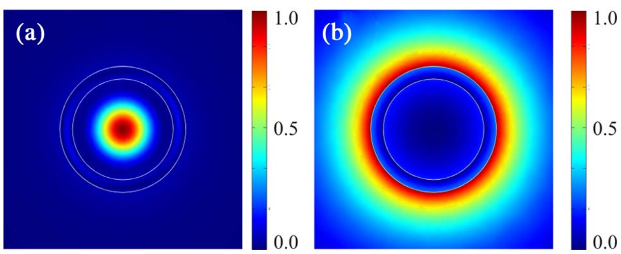

Fig. 9. (Color online) Longitudinal energy flux distributions for (a) ARROW type fundamental (HE_{11} mode) in thick wall capillary (98 μm thickness, 0.95 mm diameter) at 0.57 THz, (b) total internal reflection (TIR) type mode guided by the deeply subwavelength capillary walls at 0.18 THz of the same capillary.

Finally, even thinner capillaries (wall thickness <20 μm) show a broad 0.5–0.9 THz transmission band [Fig. 10(a)] that corresponds to the TIR mode guided by the deeply subwavelength capillary walls. In Fig. 10(a) transmittance of the capillaries with 12 μm thick walls is shown for various values of the capillary length (cut-back measurements). Capillary transmission losses are low (below 0.05 cm^{-1}/19 dB/m at 0.75 THz) in the whole transmission window of 0.5–0.9 THz. Transmission measurements at different capillary length reveal the fine spectral structure, which could be a result of the structural imperfection of the capillary walls along the fiber length. The numerical simulations using the transfer matrix method give a simple explanation to the spectral position of the transmittance peak of the TIR mode. It is simply a frequency at which the overlap between the TIR mode and incoming Gaussian beam (whose waist is proportional to the wavelength) is maximized.

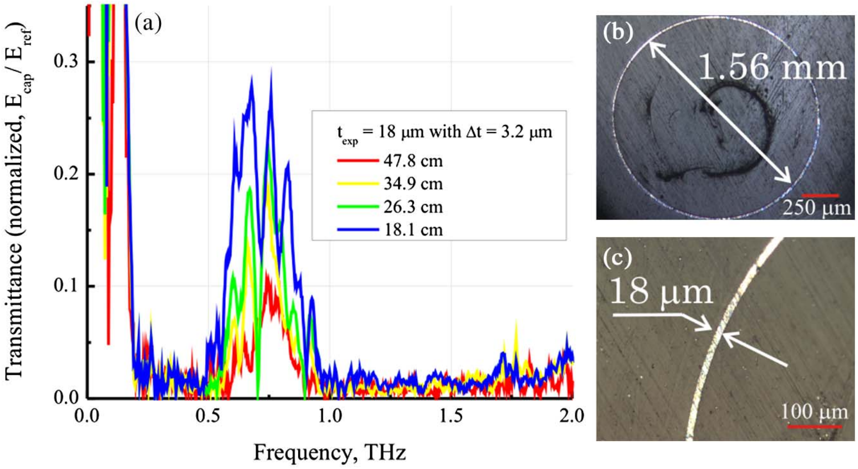

Fig. 10. (Color online) (a) Transmittance of the capillary with average wall thickness 12 μm in the 0.1–2.0 THz spectral range with ~19 dB/m transmission loss at 0.75 THz. (b),(c) Photograph of the capillary used in the experiments with outer diameter of 1.56 mm and average wall thickness 12 μm.

5. CONCLUSION

In this work we have demonstrated that chalcogenide glass $As_{38}Se_{62}$ capillaries can be used as efficient waveguides covering the whole mid-IR—THz spectral range. The capillaries are fabricated using a double crucible glass drawing technique. The wall thickness of the glass capillaries can be well controlled during drawing by using temperature and pressure parameters, thus enabling fabrication of the chalcogenide capillaries with wall thickness varying in a wide range of 12 to 130 μm. Such capillaries show low-loss transmission of the mid-IR and THz light. Particularly, in the mid-IR range, guidance is mostly governed by Fresnel reflections at the inner walls of the capillary and by the resonances in the capillary walls (ARROW guidance). Additionally, in the THz spectral range, capillaries with deeply subwavelength wall can guide via a TIR mechanism.

ACKNOWLEDGMENTS

We would like to thank CorActive Inc. for supporting this project in the framework of the Collaborative Research and Development grant from the National Science and Engineering Research Council of Canada.

REFERENCES

1. B. Bruno, S. Maurugeon, F. Charpentier, J.-L. Adam, P. Boussard, and X.-H. Zhang, "Chalcogenide glass fibers for infrared sensing and space optics," Fiber Integr. Opt. **28**, 65–80 (2009).
2. J. Heo, M. Rodrigues, S. J. Saggese, and G. H. Sigel, Jr., "Remote fiber-optic chemical sensing using evanescent—wave interactions in chalcogenide glass fibers," Appl. Opt. **30**, 3944–3951 (1991).
3. N. Granzow, S. P. Stark, M. A. Schmidt, A. S. Tverjanovich, L. Wondraczek, and P. St. J. Russell, "Supercontinuum generation in chalcogenide-silica step-index fibers," Opt. Express **19**, 21003–21010 (2011).
4. B. Ung and M. Skorobogatiy, "Chalcogenide microporous fibers for linear and nonlinear applications in the mid-infrared," Opt. Express **18**, 8647–8659 (2010).
5. N. Hô, M. C. Phillips, H. Qiao, P. J. Allen, K. Krishnaswami, B. J. Riley, T. L. Myers, and N. C. Anheier, Jr., "Single-mode low-loss chalcogenide glass waveguides for the mid-infrared," Opt. Lett. **31**, 1860–1862 (2006).
6. A. F. Kosolapov, A. D. Pryamikov, A. S. Biriukov, V. S. Shiryaev, M. S. Astapovich, G. E. Snopatin, V. G. Plotnichenko, M. F. Churbanov, and E. M. Dianov, "Demonstration of CO_2-laser power delivery through chalcogenide-glass fiber with negative-curvature hollow core," Opt. Express **19**, 25723–25728 (2011).
7. B. Temelkuran, S. D. Hart, G. Benoit, J. D. Joannopoulos, and Y. Fink, "Wavelength-scalable hollow optical fibres with large photonic bandgaps for CO_2 laser transmission," Nature **420**, 650–653 (2002).
8. M. Zalkovskij, C. Z. Bisgaard, A. Novitsky, R. Malureanu, D. Savastru, A. Popescu, P. U. Jepsen, and A. V. Lavrinenko, "Ultrabroadband terahertz spectroscopy of chalcogenide glasses," Appl. Phys. Lett. **100**, 031901 (2012).
9. Y.-S. Jin, G.-J. Kim, and S.-G. Jeon, "Terahertz dielectric properties of polymers," J. Korean Phys. Soc. **49**, 513–517 (2006).
10. B. Ung, A. Mazhorova, A. Dupuis, M. Rozé, and M. Skorobogatiy "Polymer microstructured optical fibers for terahertz wave guiding," Opt. Express **19**, B848–B861 (2011).
11. L.-J. Chen, H.-W. Chen, T.-F. Kao, J.-Y. Lu, and C.-K. Sun, "Low-loss subwavelength plastic fiber for terahertz waveguiding," Opt. Lett. **31**, 308–310 (2006).
12. J. A. Harrington, R. George, P. Pedersen, and E. Mueller, "Hollow polycarbonate waveguides with inner Cu coatings for delivery of terahertz radiation," Opt. Express **12**, 5263–5268 (2004).
13. B. Bowden, J. A. Harrington, and O. Mitrofanov, "Silver/polystyrene-coated hollow glass waveguides for the transmission of terahertz radiation," Opt. Lett. **32**, 2945–2947 (2007).
14. T. Ito, Y. Matsuura, M. Miyagi, H. Minamide, and H. Ito, "Flexible terahertz fiber optics with low bend-induced losses," J. Opt. Soc. Am. B **24**, 1230–1235 (2007).
15. A. Dupuis, K. Stoeffler, B. Ung, C. Dubois, and M. Skorobogatiy, "Transmission measurements of hollow-core THz Bragg fibers," J. Opt. Soc. Am. B **28**, 896–907 (2011).
16. C.-H. Lai, Y.-C. Hsueh, H.-W. Chen, Y.-J. Huang, H. Chang, and C.-K. Sun, "Low-index terahertz pipe waveguides," Opt. Lett. **34**, 3457–3459 (2009).
17. C.-H. Lai, B. You, J.-Y. Lu, T.-A. Liu, J.-L. Peng, C.-K. Sun, and H. Chang, "Modal characteristics of antiresonant reflecting pipe waveguides for terahertz waveguiding," Opt. Express **18**, 309–322 (2010).
18. Y. Matsuura, R. Kasahara, T. Katagiri, and M. Miyagi, "Hollow infrared fibers fabricated by glass-drawing technique," Opt. Express **10**, 488–492 (2002).
19. M. Miyagi and S. Nishida, "Transmission characteristics of dielectric tube leaky waveguide," IEEE Trans. Microw. Theory Tech. **28**, 536–541 (1980).
20. M. Nagel, A. Marchewka, and H. Kurz, "Low-index discontinuity terahertz waveguides," Opt. Express **14**, 9944–9954 (2006).

21. E. Nguema, D. Férachou, G. Humbert, J.-L. Auguste, and J.-M. Blondy, "Broadband terahertz transmission within the air channel of thin-wall pipe," Opt. Lett. **36**, 1782–1784 (2011).
22. D. Chen and H. Chen, "A novel low-loss terahertz waveguide: Polymer tube," Opt. Express **18**, 3762–3767 (2010).
23. M. Naftaly and R. E. Miles, "Terahertz time-domain spectroscopy: A new tool for the study of glasses in the far infrared" J. Non-Cryst. Solids **351**, 3341–3346 (2005).
24. T. Kanamori, Y. Terunuma, S. Takahashi, and T. Miyashita, "Chalcogenide glass fibers for mid-infrared transmission," J. Lightwave Technol. **2**, 607–613 (1984).
25. R. Mossadegh, J. S. Sanghera, D. Schaafsma, B. J. Cole, V. Q. Nguyen, R. E. Miklos, and I. D. Aggarwal, "Fabrication of single-mode chalcogenide optical fiber," J. Lightwave Technol. **16**, 214–217 (1998).
26. V. S. Shiryaev, J.-L. Adam, X. H. Zhang, C. Boussard-Pledel, J. Lucas, and M. F. Churbanov, "Infrared fibers based on Te–As–Se glass system with low optical losses," J. Non-Cryst. Solids **336**, 113–119 (2004).
27. M. F. Churbanov, "High-purity chalcogenide glasses as materials for fiber optics," J. Non-Cryst. Solids **184**, 25–29 (1995).
28. M. F. Churbanov, G. E. Snopatin, V. S. Shiryaev, V. G. Plotnichenko, and E. M. Dianov, "Recent advances in preparation of high-purity glasses based on arsenic chalcogenides for fiber optics," J. Non-Cryst. Solids **357**, 2352–2357 (2011).
29. V. S. Shiryaev, S. V. Smetanin, D. K. Ovchinnikov, M. F. Churbanov, E. B. Krukova, and V. G. Plotnichenko, "Effect of impurities of oxygen and carbon on optical transparency of As_2Se_3 glass," Inorg. Mater. **41**, 308–314 (2005).
30. G. E. Snopatin, V. S. Shiryaev, G. E. Plotnichenko, E. M. Dianov, and M. F. Churbanov, "High-purity chalcogenide glasses for fiber optics," Inorg. Mater. **45**, 1439–1460 (2009).
31. Amorphous Materials, "AMTIR-2: Arsenic Selenide Glass As–Se" (Amorphous Materials Inc., 2009). http://www.amorphousmaterials.com/
32. M. Roze, B. Ung, A. Mazhorova, M. Walther, and M. Skorobogatiy, "Suspended core subwavelength fibers: towards practical designs for low-loss terahertz guidance," Opt. Express **19**, 9127–9138 (2011).
33. A. Dupuis, A. Mazhorova, F. Desevedavy, M. Roze, and M. Skorobogatiy, "Spectral characterization of porous dielectric subwavelength THz fibers fabricated using a microstructured molding technique," Opt. Express **18**, 13813–13828 (2010).